

STARLESS CORES

Mario Tafalla

Observatorio Astronómico Nacional, Alfonso XII 3, E-28014 Madrid, Spain

m.tafalla@oan.es

Abstract Dense low mass cores in nearby clouds like Taurus and Auriga are some of the simplest sites currently forming stars like our Sun. Because of their simplicity and proximity, dense cores offer the clearest view of the different phases of star formation, in particular the conditions prior to the onset of gravitational collapse. Thanks to the combined analysis of the emission from molecular lines and the emission/absorption from dust grains, the last several years have seen a very rapid progress in our understanding of the structure and chemical composition of starless cores. Previous contradictions between molecular tracers are now understood to arise from core chemical inhomogeneities, which are caused by the selective freeze out of molecules onto cold dust grains. The analysis of the dust emission and absorption, in addition, has allowed us to derive accurate density profiles, and has made finally possible to carry out self consistent modeling of the internal structure of starless cores. In this paper I briefly review the evolution of core studies previous to the current golden age, and show how multi-tracer emission can now be modeled in a systematic manner. Finally I show how we can start to reconstruct the early history of core formation taking advantage of the chemical changes in the gas.

1. Introduction

Dense starless cores in nearby clouds like Taurus and Auriga represent the simplest star-forming sites. They collapse and produce individual stars (or binaries) in almost isolation, with apparently little influence from the surrounding cloud or from previous generations of stars. For this simplicity and proximity, starless cores constitute ideal places to elucidate the still mysterious process by which interstellar matter collapses and forms gravitationally-bound self-luminous objects.

The simplicity of star-formation in cores, unfortunately, comes at the price of missing some elements of interest for this meeting, like clustering or the formation of high-mass stars. Several reviews in this book provide information on these topics, and the reader is referred to them to complement the mate-

rial presented here. Despite the above limitations, however, protostars formed in starless cores display most phenomena that we associate with the birth of a typical star. Gravitational motions, binary and disk formation, and bipolar outflow ejection all occur in young stellar objects (YSOs) recently formed (or in the process of formation) in low mass cores, and most of these phenomena were in fact first identified in dense core environments. Thus, if we are to understand the basic principles and time evolution of most star-formation physics, studying dense cores offers a most promising approach.

When we observe a starless core, we are seeing a system that very likely will collapse to form a star (it is still an open question whether all starless cores are truly pre stellar). For this reason starless cores offer a snapshot of the initial conditions of star formation, and even of the first stages of the process if they have already started to collapse. Deriving these conditions from observations is therefore of great interest, and more than two decades of dense core studies attest the enormous effort made in this direction. For a number of reasons discussed below, the last five years or so have witnessed a very rapid progress in the study of dense cores, and numerous results and papers have appeared in the literature. In this contribution I review some of this recent work, with emphasis on the study of the internal structure of dense cores. In the pedagogical spirit of the workshop, I start with a brief review of the field. I have chosen a historical point of view (my own simplistic summary of the history) to emphasize what we have learned, what are some of the most relevant papers in the field, and where should be aiming to go in the future. Contributions in this book by Malcolm Walmsley and Paola Caselli treat related topics from different points of view and are highly recommended.

2. “Classical” studies of starless cores

The systematic study of low mass dense cores has a tradition of more than two decades, and starts in earnest with the first searches based on the optical inspection of Palomar Survey plates by Myers et al. (1983) (see Lee & Myers 1999 for an update of this work). These searches were followed by radio studies of their molecular emission, mostly NH_3 (e.g., Myers & Benson 1983), to determine the basic gas physical properties. Subsequent correlation of dense core positions and the location of IRAS point sources by Beichman et al. (1986) confirmed that dense cores are the sites of ongoing star formation. IRAS and NIR observations, in addition, gave rise to a division of cores into star-containing and starless, depending on whether they harbored or not a central luminous object. It should be emphasized, however, that this classical distinction is based on a given level of sensitivity achieved more than a decade ago, and estimated by Myers et al. (1987) as corresponding to a luminosity of $0.1 L_{\odot}$ for the distance of Taurus. The recent revolution in mid IR sensitivity

brought by the Spitzer Space Telescope has forced some corrections in the old classification of cores, and moved some cores previously classified as starless to the star-containing category (Young et al. 2004). The distinction between starless and star-containing cores, however, is still a fundamental one, in the sense that it distinguishes between before and after the formation of a central object.

The 1980s represent the golden years of mapping and analysis of dense cores based on their molecular line emission, what we could call the "classical period". The main results from this decade are summarized in the monumental paper by Benson & Myers (1989), whose 15th birthday closely coincides with the celebration of this meeting in October 2004. Benson & Myers's work is based on arcminute-resolution observations of a single tracer (NH_3), and concentrates on the global or average properties of cores. After observing and analyzing more than 100 dense cores (both starless and star-containing), these authors derive, among other properties, typical masses of a few M_\odot , sizes of about 0.1 pc, densities of a few 10^4 cm^{-3} , temperatures of 10 K, and subsonic turbulent motions. To recognize the importance of these results one only needs to notice that these observational parameters constituted part of the input for the so-called standard model of star formation, which crystallized almost at the same time (Shu, Adams, & Lizano 1987).

The above set of dense core properties was not free from contradictions, as already discussed in the almost simultaneous paper by Zhou et al. (1989). These authors compared observations of cores in two high density tracers, CS and NH_3 , and found systematic discrepancies between them. The most severe discrepancies were a mismatch in the position of the emission peaks of the two molecules, a factor of 2 larger size of the CS maps, and a factor of 2 broader CS lines. Although different mechanisms were invoked at the time to explain these CS/ NH_3 discrepancies, the lack of a detailed picture of the internal structure of dense cores left the problem unsolved. As we will see below, only now, after more than a decade of work by a large number of researchers, we can claim a reasonable understanding of the internal properties of starless cores and finally put an end to the old contradiction between different tracers.

3. Starless cores studies in the 1990s

The 1990s witnessed an enormous progress in the characterization of dense cores in general and starless cores in particular. This progress resulted from a decade of improvements in the techniques to trace the gas and dust components of dense cores, and in the parallel development of sophisticated tools to analyze the data. The classical method of molecular-line tracing greatly benefited from the factor of several increase in spatial resolution afforded by the new generation of millimeter and submillimeter telescopes like the IRAM 30m

and the JCMT. It also benefited from the advent of multipixel receiver arrays, like QUARRY and SEQUOIA at FCRAO, which have allowed the systematic mapping of large areas at moderate resolution. As a result, it is now possible to map and resolve large numbers of dense cores in relatively short amounts of time (e.g., Caselli et al. 2002).

More important than the incremental increase in our ability to trace the molecular emission of cores has been the development of new techniques to sample the dust component. This component can be traced by its millimeter and submillimeter thermal emission, which is optically thin and most likely arises from dust of close to constant emission properties. Pioneer work using mm and submm continuum observations has provided the first realistic density profiles of starless cores, and has shown that they present a characteristic flattening at their center (Ward-Thompson et al. 1994, Andre et al. 1996). Such a flattening implies that the dust (and gas) density in the inner 5,000-10,000 AU of a core has a close-to-constant value which typically ranges between 10^5 to 10^6 cm^{-3} (Ward-Thompson et al. 1999).

Additional progress in the tracing of the dust component comes from the technique of NIR extinction measurement, which uses the reddening of background stars behind a core or a cloud to estimate the dust column density (Lada et al. 1994). Using this technique, Alves et al. (2001) has produced an extremely detailed view of the B68 globule, and has shown that its density profile is very close to that expected for a close-to-critical isothermal (Bonnor-Ebert) sphere. A related technique, which uses the extinction by a core of the mid-IR diffuse background, has been used by Bacmann et al. (2000) to complement the mm and submm continuum emission measurements by estimating density profiles and confirming the presence of central flattening.

When the above dust measurements and molecular line observations were combined to carry out a unified analysis of starless cores, it became clear that many molecules do not sample the central and densest part of the cores, but that they disappear from the gas phase most likely due to their freeze out onto cold dust grains (Kuiper et al. 1996, Kramer et al. 1999, Caselli et al. 1999, Tafalla et al. 2002). This freeze out of molecules onto grains is not only of chemical interest by itself (see Bergin & Langer 1997 for pioneer modeling), but has important consequences for dense core studies. Molecular emission is the only tool available to study gas kinematics, so the disappearance of some species at high densities imposes a significant limitation in this type of studies. As a positive aspect, the presence of selective freeze out of molecules in the central gas of dense cores helps to explain the contradictions between CS and NH_3 observations described by Zhou et al. (1989), because these two molecules behave differently at high densities: CS freezes out easily and NH_3 does not (see Tafalla et al. 2002 for further details).

The 1990s was also a decade of intense studies of dense core kinematics, spurred by the identification of infall motions in the star-containing core B335 (Zhou et al. 1993). Among starless cores, L1544 was the first one found to present evidence for inward motions (Myers et al. 1996, Tafalla et al. 1998), and subsequent searches by Lee et al. (1999) have identified several additional cases. These initial infall searches were made using molecular species like CS and H₂CO, now known to freeze out at densities typical of dense core centers, so they were only sensitive to motions in the outer layers of the cores. More recent infall studies take molecular freeze out into consideration, and can therefore penetrate deeper into the gas.

4. The internal structure of the L1498 and L1517B cores

To show the level of detail currently possible in the analysis of the internal structure of starless cores, this section summarizes the recent study of two cores in the Taurus-Auriga complex, L1498 and L1517B. These two cores (Fig. 1) were selected for their close-to-round shape and relative isolation, in addition to being starless (no IRAS or 2MASS sources), and they have been subject to observations in the 1.2mm continuum and a number of molecular lines using the FCRAO 14m, IRAM 30m and Effelsberg 100m telescopes (Fig. 2). A complete account of this work is presented in Tafalla et al. (2004; 2005, in preparation).

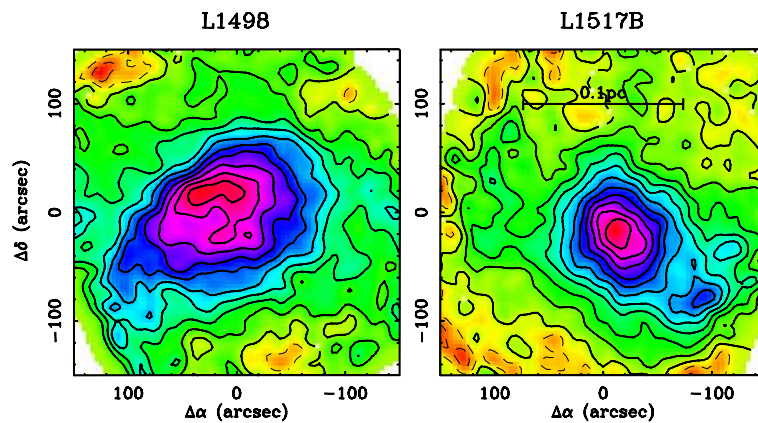


Figure 1. 1.2mm continuum maps of L1498 and L1517B. Note their central concentration and close-to-round geometries. First contour and contour spacing are 2 mJy/11''-beam.

Characterizing the internal structure of a dense core implies deriving both its physical parameters (density, temperature, turbulence) and its chemical properties (molecular abundances) as a function of position. Given that we only see the cores projected on the plane of the sky, we need to make an assumption

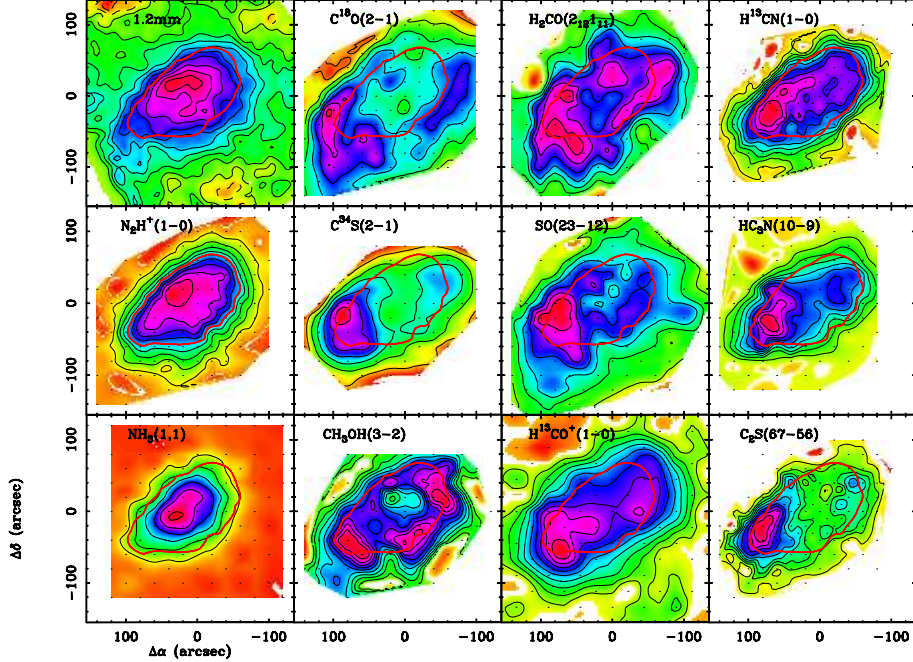


Figure 2. Sample of molecular emission maps of the L1498 core. Only the maps in the first column show centrally peaked emission, while the rest present a dip indicative of molecular depletion. For easier inter comparison, the half maximum contour of the $\text{N}_2\text{H}^+(1-0)$ emission has been superposed to each map (red line in the color version of the figure).

on their third (line-of-sight) dimension, and for the close-to-round targets of our study, we will assume spherical symmetry. Once we have fixed the geometry, we can use the optically thin 1.2mm continuum emission to derive a density profile, and the observations of appropriate molecular lines to derive the gas temperature, turbulence, and systemic motions in addition to the abundance profiles of each species. Because of the gradient in gas excitation caused by the density gradient, a non-LTE radiative transfer solution is necessary to model the molecular emission. For this work, we use the Monte Carlo radiative transfer code of Bernes (1979) updated with the most recent molecular parameters and collision rates. This model is spherically symmetric, so we compare its results with radial averages of the emission, and fit simultaneously the radial profile of integrated intensity and the central spectrum for each line. The following subsections show the analysis step by step and the conclusions derived from it.

Density

The first step in our analysis consists of deriving the density profile of each core based on its 1.2mm continuum emission. Unfortunately, this step is the most uncertain one, due to our incomplete knowledge of the physical properties of the emitting dust. In the optically thin case (a good approximation at 1.2mm), the dust emission depends on the product of the dust emissivity and the Planck function at the dust temperature, and both emissivity and dust temperature are not well constrained. For this work, we assume that the two parameters have constant values of 0.005 cm g^{-1} and 10 K, respectively. Our choice of dust temperature is based on our estimate of the gas temperature using NH_3 and presented in the next section, while our choice of emissivity follows the standard value in the literature (e.g., Andre et al. 1996). If grain growth via coagulation is important toward the core center, the true emissivity can increase there, and be larger than our assumed value by a factor of about two (Ossenkopf & Henning 1994). The dust temperature, on the other hand, may decrease toward the center due to the extinction of the interstellar radiation field (the dominant heating mechanism for dust in core environments), so it may reach a lower value of around 8 K for our cores (Evans et al. 2001, Zucconi et al. 2001, Galli et al. 2002). Thus, if for example we use an emissivity of 0.009 cm g^{-1} , as recommended by Ossenkopf & Henning (1994) (their OH5 value), and a dust temperature of 8.7 K, as derived by Galli et al. (2002) for a core similar to L1517B, we will have to decrease our densities by a factor 0.7. Our chosen values, therefore represent a simplification of the complex dust physics, but their product seems more immune to this physics than each of the individual components.

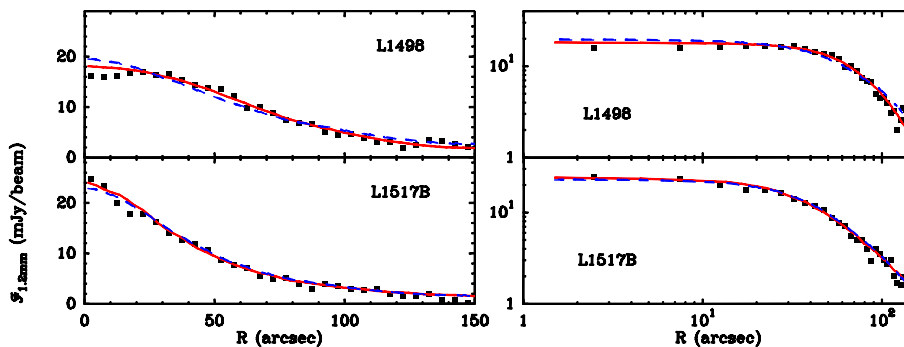


Figure 3. Radial profiles of 1.2mm continuum emission in linear-linear and log-log scales (left and right, respectively). The squares represent bolometer observations, the solid lines are the predictions from an analytic model, and the dashed line are the predictions from an isothermal model (see text).

Once we have chosen the dust parameters, we can invert the observed emission into a density profile. To do this, we start with a choice of density distribution and predict its expected emission by solving the equation of radiative transfer and simulating an on-the-fly observation with a bolometer array (including secondary chopping). The result of this prediction is compared with the observed radial profile, and the density distribution is corrected accordingly; the process is repeated until the model matches the observations. As density profiles, we have used two families of curves. One is the empirical formula

$$n(r) = n_0 / (1 + (r/r_0)^\alpha),$$

where n_0 , r_0 , and α are free parameters that correspond to the central density, half maximum radius, and asymptotic power law of the density profile. Note that this profile contains naturally the central flattening first found by Ward-Thompson et al. (1994). The other family of density profiles is the family of isothermal (Bonnor-Ebert) profiles, which has only two free parameters, the central density and the effective sound speed.

The result from the fitting procedure is shown in Figure 3, where both linear-linear and log-log radial profiles of the observed 1.2mm intensity (squares) are shown together with the predictions from the analytic (solid lines) and isothermal (dashed-lines) models. As can be seen, both families of models fit similarly well the data, with the analytic model for L1498 fitting slightly better the profile than the isothermal model. Both families of models require similar central densities, 10^5 cm^{-3} for L1498 and $2 \cdot 10^5 \text{ cm}^{-3}$ for L1517B, and the size of the half maximum radius (from the analytic model) is approximately 10,000 AU for L1498 and 5,000 AU for L1517B. L1498, therefore, is slightly less dense and more extended than L1517B, but both cores have similar central column densities: $3\text{-}4 \times 10^{22} \text{ cm}^{-2}$ (30-40 A_v). With respect to the α parameter, we derive 3.5 and 2.5 for L1498 and L1517B, respectively. The 2.5 value for L1517B makes the analytic fit indistinguishable from isothermal fit, as it can be shown that the analytic formula becomes an excellent approximation to the Bonnor-Ebert sphere for the case of $\alpha = 2.5$ (see Tafalla et al. 2004, Appendix B).

Temperature

To derive the gas temperature profiles of L1498 and L1517B, we use $\text{NH}_3(1,1)$ and $(2,2)$ observations. The combined analysis of these two lines can provide a reliable and straightforward estimate of the gas kinetic temperature with minimal assumptions, and to achieve that, we have updated the classical NH_3 analysis of Walmsley & Ungeretchs (1983) using a Monte Carlo radiative transfer solution. The derived radial profiles of gas kinetic temperature are shown in

Figure 4 (left panel), and for both cores are relatively flat with a constant value of 10 K.

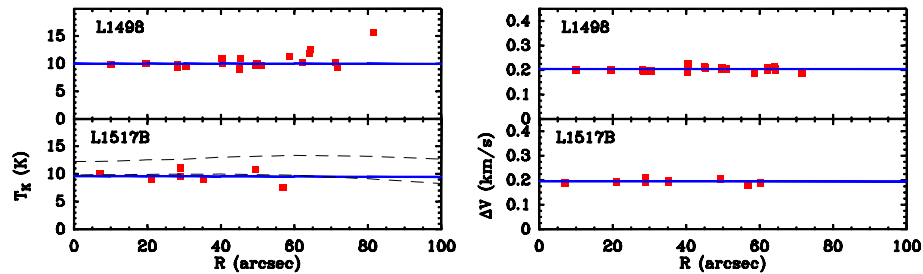


Figure 4. *Left:* radial profiles of gas kinetic temperature as derived from the analysis of the NH_3 emission. The solid lines are constant temperature fits at 10 K and the dashed lines are the predictions from two models by Galli et al. (2002). *Right:* radial profiles of total NH_3 linewidth as derived from a hyperfine analysis to the (1,1) spectrum. The lines represent two constant linewidth fits with $\Delta V = 0.2 \text{ km s}^{-1}$.

At the central gas densities of L1498 and L1517B, dust and gas are expected to be thermally coupled, and therefore follow similar gradients with radius. As mentioned before, the dust kinetic temperature is expected to drop towards the core center (Evans et al. 2001, Zucconi et al. 2001), but our gas temperature profiles do not show such a trend. Our NH_3 observations have a $40''$ resolution (FWHM), so it is still possible to hide a small temperature gradient, but not a very large one given the strong weight of the NH_3 emission towards the core center due to its higher abundance there (see below). To test our sensitivity to a temperature gradient, we have used the realistic temperature profiles predicted by Galli et al. (2002) for a core very similar to L1517B, and simulated an NH_3 observation with $40''$ resolution followed by a temperature analysis. The results, shown as dashed lines in Fig. 4, indicate that to fit the data, a low cosmic rate is needed (1/5 of standard), and that for this case, which has a central drop of about 1 K, the fit is as good as the constant temperature fit. The central gas temperature in L1517B, therefore, may be slightly lower than in the outside, but not by much more than 1 K. Such a strong constrain arises from the strong sensitivity to temperature of the $\text{NH}_3(2,2)$, whose intensity would double by just increasing the temperature by 3 K.

Turbulence

The NH_3 lines also provide a sensitive measure of the gas turbulent motions via the hyperfine analysis of the (1,1) spectra. Figure 5 (right panel) presents the radial profiles of total NH_3 linewidth (FWHM) for L1498 and L1517B, which are again flat with a constant value of 0.2 km s^{-1} and a very small

dispersion ($\leq 0.01 \text{ km s}^{-1}$, consistent with random errors). This constant linewidth with radius is in contrast with the so-called linewidth-size relation (e.g., Larson 1981) in two ways. First, the linewidth does not increase with radius, and second, the linewidth of the more extended L1498 core is the same as that of the more compact L1517B. The lack of linewidth increase with radius in dense cores has been discussed in detail by Goodman et al. (1998).

The total linewidth represented in Figure 4 is the harmonic average of a thermal and a non-thermal components. For NH_3 molecules at 10 K, the thermal component is 0.16 km s^{-1} , so this component dominates the linewidth, while the turbulent component is subthermal (see also Myers 1983). To compare the contribution of the two components to the equilibrium of the core, we take the ratio between thermal and non-thermal pressures:

$$\frac{P_{NT}}{P_T} = \frac{\sigma_{NT}^2}{kT/m} \approx 0.07,$$

where σ_{NT} is the turbulent component ($= \Delta V / \sqrt{8 \ln 2} = 0.05 \text{ km s}^{-1}$) and m is the mean particle mass (2.33 the proton mass). As the ratio indicates, the contribution of the turbulent component to the support of the core is negligible in the central 0.1 pc.

Molecular composition

Once the density, temperature and kinematics of the cores have been determined, the only free parameter we can adjust to model the observed emission of any molecule is the abundance profile of that species (see Tafalla et al. 2004 for a discussion on the velocity fields in L1498 and L1517B, omitted here for lack of space). This means that we can use the L1498 and L1517B cores as laboratories of known physical properties to measure the behavior of molecules at high densities and determine their sensitivity to freeze out onto dust grains. In order to simplify the modeling and the comparison between molecules, we use for all species an abundance profile with a constant value of X_0 at large radius and a step central hole at R_{hole} (NH_3 has a central increase). For each species at least two transitions have been observed, and for each of them we model simultaneously both its radial profile of integrated intensity and its central emerging spectrum. This is done with a Monte Carlo radiative transfer code (Bernes 1979) together with a convolution routine to simulate an astronomical observation.

A summary of the modeling results is presented in Figure 5, where the radial profiles for one transition of each species in L1498 are shown (squares) together with the best fit model (solid line) and a model with constant abundance equal to the outer value of the best fit model (dashed lines). As can be seen, all molecules but N_2H^+ and NH_3 require a central abundance hole of

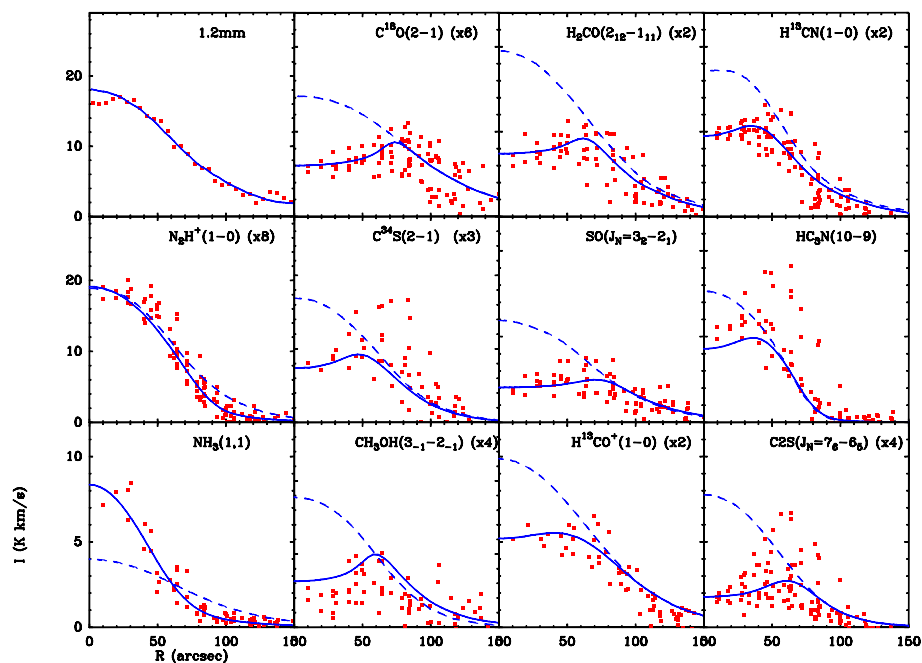


Figure 5. Radial profiles of emission from L1498 for the tracers shown in Figure 2. The squares represent observations, the dashed lines are the predictions from constant abundance models set to fit the outer emission, and the solid lines are the best fit models (they also fit additional lines not shown here). For all species in the second, third, and fourth columns, the best fit models contain a central abundance hole.

variable size (5,000-10,000 AU), which indicates that they freeze out at densities of a few 10^4 cm^{-3} . A similar behavior is found in L1517B.

The above pattern of abundances in L1498 and L1517B is in general agreement with recent models of starless core chemistry, which show that only species based on the simplest nitrogen chemistry can survive for a significant time at densities of 10^5 cm^{-3} (e.g., Bergin & Langer 1997, Shematovich et al. 2003, Aikawa et al. 2003). This behavior results from a combination of the lower binding energy of the N_2 molecule to dust grains, which allows N chemistry to proceed at high densities, together with the favorable chemistry resulting from the disappearance of CO from the gas phase (see chapter by Paola Caselli in this volume for more details). Although the general agreement between models and observations is good, there are still some puzzling behaviors, like the abundance increase of NH_3 at high densities while the abundance of its cousin species N_2H^+ stays constant. Further modeling of the high density core chemistry is still needed to explain the data (see Aikawa et al. 2005).

From the point of view of observations, the results from L1498 and L1517B are a strong reminder that very few molecules survive in the gas phase at the typical densities of a starless core. Extreme care should therefore be exercised when choosing a molecular tracer to study the properties of the star-forming material in these environments.

5. Tracing core evolution with molecular freeze out

Our new understanding of molecular freeze out is finally allowing a self consistent picture of core interiors to emerge. It also promises to shed crucial light on the still mysterious process of core contraction. This is so because molecular freeze out is a progressive and irreversible process at the densities and temperatures of starless cores. Each molecule that hits a dust grain under these conditions will stick to its surface and will not evaporate thermally (cosmic ray-induced evaporation seems not efficient enough to reverse the process, see Leger et al. 1985, Hasegawa & Herbst 1993). The amount of freeze out in a given parcel of gas, therefore, will increase with time, and it should be possible in principle to convert the amount of freeze out into an estimate of the contraction age. In practice, unfortunately, this is not yet achievable because of the uncertainties in the binding energies of molecules to dust grains (but see Aikawa et al. 2005 for a recent detailed modeling). Molecular freeze out, however, can already be used as a qualitative time marker thanks to the simple fact that it increases with time. This means that by looking at the amount of freeze out of a sensitive molecule (like CO or CS), we can distinguish cores at different contraction stages, although we cannot yet assign them a particular age.

Molecular freeze out is not the only process that increases with time in a contracting core. Some molecules like NH_3 and N_2H^+ gradually become more abundant because their formation depends on the slow formation of N_2 (e.g., Suzuki et al. 1992), so they are also useful indicators of core evolution (N_2H^+ is further enhanced by the depletion of CO). Thus, we can expect that a core starts its life being CO/CS rich at its center (not enough time to freeze out) and $\text{NH}_3/\text{N}_2\text{H}^+$ poor (not enough time to form N_2) and evolves toward being centrally CO/CS poor (due to freeze out) and $\text{NH}_3/\text{N}_2\text{H}^+$ rich (due to late-time chemistry). To quantify this trend, we define a ratio between the intensities of two molecules with opposite behaviors. For observational convenience, we chose the two thin species C^{18}O and N_2H^+ , as they have $J=1-0$ transitions at 3mm, and can therefore be observed with the same telescope at similar resolutions. Thus, we define

$$R = I[\text{C}^{18}\text{O}(1-0)] / I[\text{N}_2\text{H}^+(1-0)],$$

where both integrated intensities are measured at the core center (as defined by the mm continuum peak). A young core is expected to have strong C^{18}O

emission and weak N_2H^+ emission, so it will be characterized by a relative large value of R . Conversely, an evolved core will be weak in C^{18}O and bright in N_2H^+ , so its R ratio will be low. Using typical abundances of C^{18}O and N_2H^+ in dense cores (Tafalla et al. 2004), we estimate that the dividing line between young and evolved cores occurs at about $R = 1$.

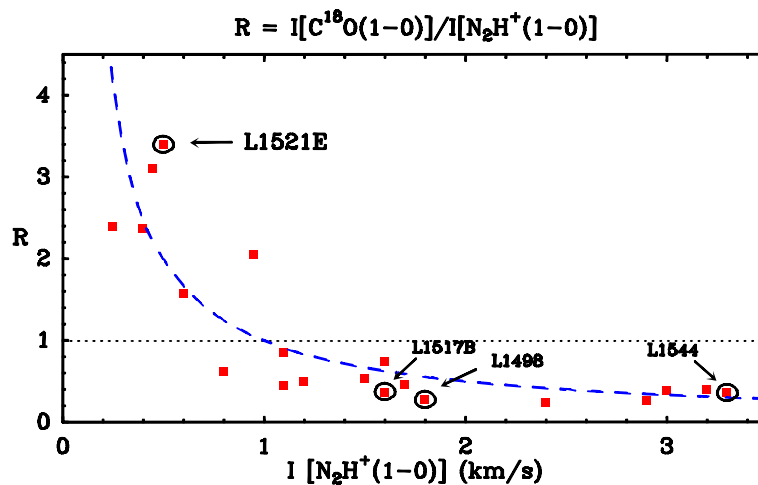


Figure 6. Plot of the R factor ($R = I[\text{C}^{18}\text{O}(1-0)]/I[\text{N}_2\text{H}^+(1-0)]$) as a function of $\text{N}_2\text{H}^+(1-0)$ intensity for a sample of starless cores. This factor seems to be an indicator of core evolution, and to decrease as a core ages. The positions of the extremely young core L1521E, the intermediate-age cores L1498 and L1517B, and the highly evolved L1544 are indicated. The dashed line is the prediction from a simplified model of core evolution.

Figure 6 presents a plot of the R ratio as a function of $\text{N}_2\text{H}^+(1-0)$ central intensity for a sample of 21 starless cores. Most cores lie below the $R = 1$ line, suggesting that C^{18}O is frozen out at their center, a fact confirmed by Monte Carlo radiative transfer calculations for some of them (L1498, L1517B, L1544, see Tafalla et al. 2002). As these cores were selected from NH_3 surveys (like that of Benson & Myers 1989), the presence of freeze out at their center is an indication that they belong to a population of objects already chemically evolved, and therefore relatively “old” (of course, not old enough to have formed a star).

In order to find cores with a ratio $R > 1$ indicative of chemical youth, we have selected starless cores known to have weak or undetected NH_3 emission, and we have mapped them in C^{18}O and N_2H^+ with the 14m FCRAO telescope (Tafalla et al. 2005, in preparation). As a result of this search, we have identified a small population of starless cores with $R > 1$, which at the same time have a relatively low value of $I[\text{N}_2\text{H}^+(1-0)]$. These cores populate the upper-left region of the diagram in Fig. 6, and represent the best candidates for

chemically young starless cores. The object with largest R value is L1521E in Taurus, and because of its extreme characteristics, it has been the subject of a more detailed study.

L1521E: the youngest starless core?

To understand the origin of the extreme R value in L1521E, we have observed this core with high resolution using the IRAM 30m telescope (see Tafalla & Santiago 2004 for a full report). These observations have been made in the 1.2mm continuum, $\text{N}_2\text{H}^+(1-0)$, and several rare isotopes of CO, and the results have been analyzed with the same method as the L1498 and L1517B data presented in section 4. A gas and dust kinetic temperature of 10 K has been assumed, as suggested by the observations of (very weak) NH_3 lines with the Effelsberg 100m telescope.

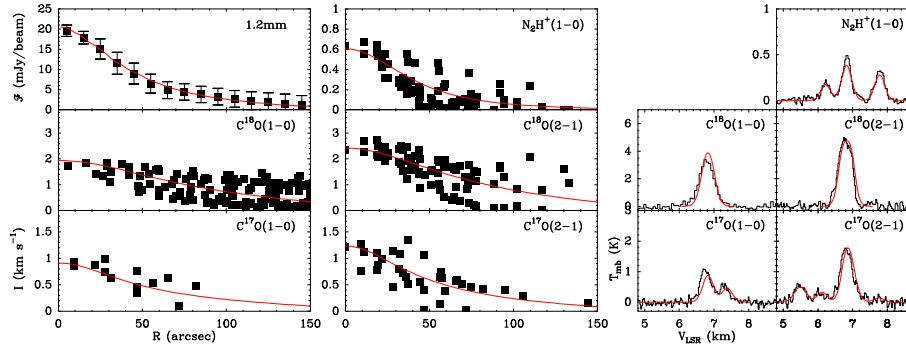


Figure 7. Radial profiles of integrated intensity (left) and emerging spectra (right) of different tracers towards L1521E. The squares and histograms are observed data, and the lines are model predictions. In contrast with the results from the L1498 analysis (Figure 5), the CO isotopomer emission from L1521E can be fit with a constant abundance model. This makes L1521E the first starless cores with negligible CO depletion.

The main results of the L1521E analysis are summarized in Fig. 7, which shows radial profiles of integrated intensity and emerging central spectra for all our data. As in the L1498 and L1517B analysis, the squares represent the observed data and the lines are fits from a Monte Carlo radiative transfer calculation (or an optically thin analysis for the 1.2mm continuum). In contrast with the L1498 and L1517B cores, however, all CO isotopomer data from L1521E can be fit assuming a constant abundance, together with a $\text{C}^{18}\text{O}/\text{C}^{17}\text{O}$ isotopic ratio of 3.65 (Penzias 1981). In addition, the value of the C^{18}O abundance in L1521E is almost the same as the value needed to fit the outer part of the L1498 and L1517B cores. This all suggests that C^{18}O is not frozen out at the center of L1521E, or if it is, it happens only in a very small region diluted by

our resolution and sampling (about $20''$). In this respect, L1521E is the first starless core consistent with no freeze out.

The very large R value of L1521E ($R = 3.4$) not only arises from a lack of significant $C^{18}O$ depletion. It also results from a very low value of its N_2H^+ abundance, which according to the Monte Carlo calculations is 8 times lower than that estimated for L1498 and L1517B. As mentioned before, a low N_2H^+ abundance is another indication of extreme youth given the late-time character of this species. More evidence for a L1521E being a young core comes from previous work by Suzuki et al. (1992) and Hirota et al. (2002), who also concluded that L1521E is unusually young based in its very bright CS and C_2S emission and its weak NH_3 lines. It is reassuring that all these different lines of work consistently indicate that the L1521E core is unusually chemically unprocessed.

Given the multiple indications of chemical youth, it is surprising that the density profile of L1521E is very similar to that of more evolved cores like L1517B. At least naively, one would have expected that a young core should have a lower central density and a more distended (cloud-like) structure, but clearly this is not the case for L1521E. Whether this is unique to this core (as a the result of fast contraction) or typical of all young cores requires the study of more objects that lie above the $R = 1$ line in Figure 6. Work currently in progress will hopefully answer this question soon.

Acknowledgments

It is a pleasure to thank the organizers of this workshop, especially Nanda Kumar, for an enjoyable and productive meeting. Part of the work presented here is the result of an ongoing collaboration with Joaquin Santiago, Phil Myers, Paola Caselli, Malcolm Walmsley, and Claudia Comito. I thank them warmly for help and many discussions on starless cores and related issues over the last several years.

References

- Aikawa, Y., Ohashi, N., Herbst, E. 2003, ApJ, 593, 906
 Aikawa, Y., Herbst, E., Roberts, H., & Caselli, P. 2005, ApJ, 620, 330
 Alves, J.F., Lada, C.J., & Lada, E.A. 2001, Nature, 409, 159
 Andre, P., Ward-Thompson, D., & Motte, F. 1996, A&A, 314, 625
 Bacmann, A., Andre, P., Puget, J.-L., Abergel, A., Bontemps, S., & Ward-Thompson, 2000, A&A, 361, 558
 Beichman, C.A., Myers, P.C., Emerson, J.P., Harris, S., Mathieu, R., Benson, P.J., & Jennings, R.E. 1986, ApJ, 307, 337
 Benson, P.J. & Myers, P.C. 1989, ApJS, 71, 89
 Bergin, E.A. & Langer, W.D. 1997, ApJ, 486, 316
 Bernes, C. 1979, A&A, 73, 67
 Caselli, P., Benson, P.J., Myers, P.C., Tafalla, M., 2002, ApJ, 572, 238

- Caselli, P., Walmsley, C.M., Tafalla, M., Dore, L., & Myers, P.C. 1999, ApJ, 523, L165
- Evans, N.J.,II., Rawlings, J.M.C., Shirley, Y.L., Mundy, L.G. 2001, ApJ, 557, 193
- Galli, D., Walmsley, C.M., & Goncalves, J. 2002, A&A, 394, 275
- Goodman, A.A., Barranco, J., Wilner, D.J., & Heyer, M.H. 1998, ApJ, 504, 223
- Hasegawa, T.I. & Herbst, E. 1993, MNRAS, 261, 83
- Hirota, T., Ito, T., & Yamamoto, S. 2002, ApJ, 565, 359
- Kramer, C., Alves, J., Lada, C.J., Lada, E.A., Sievers, A., Ungerechts, H., Walmsley, C.M. 1999, A&A, 342, 257
- Kuiper, T.B.H., Langer, W.D., Velusamy, T. 1996, ApJ, 468, 761
- Lada, C.J., Lada, E.A., Clemens, D.P., & Bally, J. 1994, ApJ, 429, 694
- Larson, R.B. 1981, MNRAS, 194, 809
- Leger, A., Jura, M., & Omont, A. 1985, A&A, 144, 147
- Lee, C.W., & Myers, P.C. 1999, ApJS, 123, 233
- Lee, C.W., Myers, P.C. & Tafalla, M. 1999, ApJ, 526, 788
- Myers, P.C. 1983, ApJ, 270, 105
- Myers, P.C., Bachiller, R., Caselli, P., Fuller, G.A., Mardones, D., Tafalla, M., Wilner, D.J. 1996, ApJ, 449, L65
- Myers, P.C., & Benson, P.J. 1983, ApJ, 266, 309
- Myers, P.C., Linke, R.A., & Benson, P.J. 1983, ApJ, 264, 517
- Myers, P.C., Fuller, G.A., Mathieu, R.D., Beichman, C.A., Benson, P.J., Schild, R.E., Emerson, J.P. 1987, ApJ, 319, 340
- Ossenkopf, V. & Henning, T. 1994, A&A, 291, 943
- Penzias, A.A. 1981, ApJ, 249, 518
- Shematovich, V.I., Wiebe, D.S., Shustov, B.M., Li, Z.-Y. 2003, ApJ, 588, 894
- Shu, F.H., Adams, F.C., & Lizano, S. 1987, ARA&A, 25, 23
- Suzuki, H., Yamamoto, S., Ohishi, M., Kaifu, N., Ishikawa, S.-I., Hirara, Y., & Takano, S. 1992, ApJ, 392, 551
- Tafalla, M., Mardones, D., Myers, P.C., Caselli, P., Bachiller, R., & Benson, P.J. 1998, ApJ, 504, 900
- Tafalla, M., Myers, P.C., Caselli, P., Walmsley, C.M., & Comito, C. 2002, ApJ, 569, 815
- Tafalla, M., Myers, P.C., Caselli, P., & Walmsley, C.M. 2004, A&A, 416, 191
- Tafalla, M. & Santiago, J. 2004, A&A, 423, L21
- Walmsley, C.M. & Ungerechts, H. 1983, A&A, 122, 164
- Ward-Thompson, D., Motte, F., & Andre, P. 1999, MNRAS, 305, 143
- Ward-Thompson, D., Scott, P.F., Hills, R.E., Andre, P. 1994, MNRAS, 268, 276
- Young, C.H. et al. 2004, ApJS, 154, 396
- Zhou, S., Evans, N.J., II, Kömpe, C., Walmsley, C.M. 1993, ApJ, 404, 232
- Zhou, S., Wu, Y., Evans, N.J.,II, Fuller, G.A., & Myers, P.C. 1989, ApJ, 346, 167
- Zucconi, A., Walmsley, C.M., & Galli, D. 2001, A&A, 376, 650